Aerodynamically-assisted electrified microscopic jets

F. Cruz-Mazo,[1] M. O. Wiedorn,[2,3,4] M. A. Herrada,[1] S. Bajt,[5] H. N. Chapman,[2,3,4] and A. M. Gañán-Calvo[1]

[1] *Departamento de Ingeniería Aerospacial y Mecánica de Fluidos, Universidad de Sevilla, Camino de los Descrubrimientos s/n 41092 Sevilla, Spain.*

[2] *Center for Free-Electron Laser Science, Deutsches Elektronen-Synchrotron DESY, Notkestrasse 85, 22607 Hamburg, Germany.*

[3] *Department of Physics, University of Hamburg, Luruper Chaussee 149, 22761 Hamburg, Germany.*

[4] *The Hamburg Center for Ultrafast Imaging, University of Hamburg, Luruper Chaussee 149, 22761 Hamburg, Germany.*

[5] *Deutsches Elektronen-Synchrotron DESY, Notkestrasse 85, 22607 Hamburg, Germany.*

(Dated: November 23, 2018)

We introduce a way to produce steady micro/nano-liquid jets via electrohydrodynamic fields together with co-flowing gas streams. We study the dripping-jetting transition of this configuration theoretically through a global stability analysis as a function of the governing parameters involved. A balance between the local radial acceleration to the surface tension gradient, the mass conservation and the energy balance equations enable us to derive two coupled scaling laws that predict both the minimum jet diameter and its maximum velocity. The theoretical prediction provides a single curve that describes not only the numerical computations but also experimental data from the literature for cone-jets. Additionally, we performed a set of experiments to verify what parameters influence the jet length. We adopt a very recent model for capillary jet length to our configuration by combining electrohydrodynamic effects with the gas flow through an equivalent liquid pressure. Due to the diameters below 1 micrometer and high speeds attainable in excess of 100 m/s, this concept has the potential to be utilized for structural biology analyses with X-ray free-electron lasers at megahertz repetition rates as well as other applications.

The ubiquitous study of liquid jets and drops during the last decades [1] has accompanied their increasing use in applications within analytical chemistry [2], [3] or material science [4] among others. In this sense, a prominent example is *Serial Femtosecond Crystallography* (SFX) [5], with the use of flow focusing (FF) [6],[7], [8] and electrospray (ES) [9], [10] for carrying biological samples to the region where they interact with the focused X-ray pulse [11], [12]. With the introduction of X-ray free-electron laser facilities that produce pulses at megahertz rates, even smaller and faster liquids are required [13], [14]. The interaction with each X-pulse is quite violent and influences more than just the intersecting volume of the X-ray beam with the jet. The jets need to run fast enough to introduce fresh sample on each pulse, taking into account the explosive interaction with the X-rays [15].

It is well known that smaller nozzles in flow focusing or electrospray geometry lead to tinier jets. However, miniaturization also reduces the robustness of such systems (e.g. increasing the likelihood of clogging). Thus, it is desirable to work at optimum conditions for both maximum speed v_j and minimum diameter D_j given a certain nozzle size. This entails the maximization of the driving pressure ΔP and the minimization of the liquid flow rate Q_ℓ for a steady operation, as can be noted from the established scaling laws for capillary cone-jets as a function of the flow properties and governing parameters (e.g. surface tension σ, viscosity μ_ℓ, density ρ_ℓ, electrical conductivity K, permittivity ε, gas pressure ΔP_g and electrical pressure ΔP_{ES}): $v_j \approx (2\Delta P/\rho_\ell)^{1/2}$, $D_j \approx (8\rho_\ell Q_\ell^2/\pi^2\Delta P)^{1/4}$, with $\Delta P = \Delta P_{FF} \sim \Delta P_g$ and

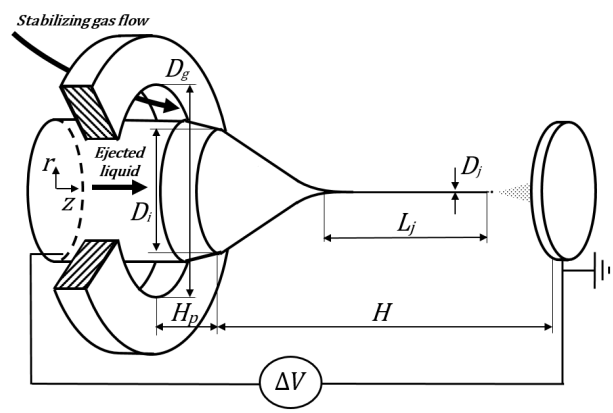

FIG. 1. Sketch of the Aerodynamically-assisted Electrified Jet nozzle

$\Delta P = \Delta P_{ES} \sim (\sigma^2 K^2 \rho_\ell/\epsilon_o^2)^{1/3}$ for flow focusing and electrospray under the dominance of inertia and electrostatic suction, respectively [16], [17]. But any accurate modeling of the jet behavior must contend with instability mechanisms within the fluid domain that may prevent the ideal steady jetting and imposes some additional constraints to the problem. So, for a given Weber number We_ℓ^* within the range $1 \lesssim We_\ell = \rho_\ell v_j^2 D_j/2\sigma \lesssim 20$, the maximum jet speed is limited by the minimum liquid flow rate Q_{min}. Consequently, we can transform this optimization problem into that of finding the dripping-jetting transition, which has been recently linked to the global stability analysis of focused liquid jets [18], [19].

We propose here a method to generate liquid jets using electrohydrodynamic forces together with co-flowing gas streams producing shear axial forces on the jet (Fig. 1). Specifically, we fluid with a flow Q_ℓ from a capillary with an inner diameter D_i. The liquid stream is forced to discharge into a low density ambient gas with an electrical permittivity close to vacuum ϵ_o. The main driver is an imposed electrical potential ΔV between the liquid capillary and a grounded electrode placed at a distance H downstream from the nozzle end. Additionally, a mass flow rate Q_{mg} of a dielectric gas with density ρ_g and viscosity μ_g is forced to flow co-axially through an annulus nozzle (Fig. 1) with a hydraulic diameter $D_g^{(h)}$ that leads to a gas Reynolds number $Re_g = Q_{mg}/\mu_g D_g^{(h)}$, with a characteristic velocity $v_g \sim Q_{mg}/\rho_g D_g^{(h)2}$. Then a steady liquid jet with a diameter D_j and an intact length L_j is issued. Each flow has a boundary layer of thickness $\delta_g \sim (\mu_g D_g^{(h)}/\rho_g v_s)^{1/2}$ and $\delta_\ell \sim (\mu_\ell D_i/\rho_\ell v_s)^{1/2}$ for the gas and liquid, respectively, with a characteristic velocity v_s. The electrical charge density in the bulk, is approximately zero owing to the electrical relaxation time of the charges $t_e \sim \epsilon/K$, which is much smaller than the characteristic hydrodynamic time $t_h \sim L_t D_j^2/Q_\ell$ along the cone-jet transition length $L_t = \epsilon_o \Delta V^2/\sigma$. At the vicinity of this region, shear electric stresses E_s are comparable to the normal electrical stress on the cone $E_n \sim (\sigma/\epsilon_o L_t)^{1/2}$, the voltage mainly decays as $\Delta V \sim E_s L_t$ and the electrical current transported by the jet turns out $I \sim K D_j^2 E_s$ [20], [21]. For conditions close to the dripping-jetting instability, the section at the stagnation point has a characteristic diameter $D_o \sim D_j$ and is located within the electrical cone-jet transition region. Between that stagnation section and where the jet emerges from the hydrodynamic transition region at a distance l downstream, mass continuity dictates that the liquid flow rate through the liquid boundary layer of thickness δ_ℓ is equal to to the liquid flow rate through the jet, leading to $v_s D_j \delta_\ell \sim v_j D_j^2$. Here, we postulate that the local radial acceleration of perturbations grows downstream through the liquid boundary layer until it becomes eventually of the same order of magnitude than the surface tension gradient at l downstream, which demands

$$\rho_\ell \frac{v_s \delta_\ell}{l t_o} \sim \frac{\sigma}{l D_j} \tag{1}$$

This temporal amplification would play the role of triggering the underlying global instability mechanisms that lead to the dripping-jetting transition within the liquid domain. Since the characteristic time of surface wave package t_o is scaled at first order as the capillary time $t_o \sim (\rho D_j^3/\sigma)^{1/2}$, the algebraic manipulation of the equation (1) and the mass balance enables us to derive the first-order estimates for $v_s \sim \sigma^2/\mu_\ell \rho_\ell D_i v_j^2$ and $D_j \sim \sigma/\rho_\ell v_j^2$. Making the later dimensionless with the intrinsic viscous-capillary length of the liquid $l_\mu = \mu_\ell^2/\rho_\ell \sigma$ and

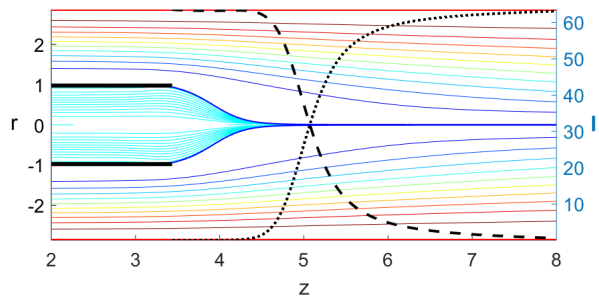

(a)

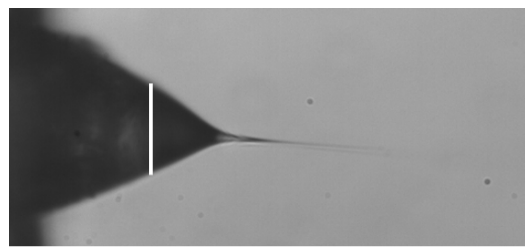

(b)

FIG. 2. (a) Numerical and (b) experimental stable flows for $4Q_\ell/\pi D_i^2 v_c = 0.023$; $Re_g = 26.7$; $C = 3.0382$; $\mu = 0.0001625$; $\rho = 0.00104167$; $\chi = 8$; $\beta = 40$; $\alpha = 124479$. The critical eigenvalue of the base flow is $0.0269 - 0.0356i$, which corresponds to about $v_j \approx 100$ m/s and $D_j \approx 200$ nm. In (a), right vertical axes is the dimensionless electrical current level I for both bulk conduction (dashed line) and surface convection (dotted line). Streamlines of both flows are plotted in each domain. In (b), the liquid cone-jet is shown to the right of the white line and the nozzle to the left.

the capillary velocity $v_\mu = \sigma/\mu_\ell$, we obtain the following relation

$$\left(\frac{v_j}{v_\mu}\right)^2 = c_d \frac{l_\mu}{D_j} \tag{2}$$

where c_d is a constant to be determined later. An energy balance closes the scaling analysis. Specifically, two power sources exist in the problem, the electrical part given by $I \cdot \Delta V \sim \sigma K D_j^2/\epsilon_o$ and the contribution from the kinetic energy of the gas flow $O(\rho_g v_g^2)$ carried by the boundary layer, whose associated flow rate $O(v_s D_j \delta_g)$ leads to a total power as $O(\rho_g v_g^2 v_s D_j \delta_g)$. These energy sources are converted by the jet in the form of kinetic energy $O(\rho_\ell v_j^3 D_j^2)$. Hence, the power balance evaluated at the dripping-jetting transition is found to be

$$c_j \widehat{v_j}^3 - c_g (\rho \mu \Upsilon_g)^{1/2} \widehat{v_g}^2 \widehat{v_j} = c_e \alpha \tag{3}$$

where we include the following dimensionless numbers $\rho = \rho_g/\rho_\ell$, $\mu = \mu_g/\mu_\ell$, $\Upsilon_g = D_g^{(h)}/D_i$, $\widehat{v_j} = v_j/v_c$, $\widehat{v_g} = v_g/v_c$, $\alpha = (\rho_\ell D_i^3 K^2/8\epsilon_o^2 \sigma)^{1/2}$ and $v_c = (2\sigma/\rho_\ell D_i)^{1/2}$. The dimensionless electrical term $c_e \alpha$ is balanced to the dimensionless kinetic energy of the jet $c_j \widehat{v_j}^3$ minus the contribution of the dimensionless kinetic energy from

the wrapping gaseous boundary layer $c_g(\rho\mu\Upsilon_g)^{1/2}\widehat{v_g}^2\widehat{v_j}$. The coefficients c_e, c_g and c_j are dimensionless numbers that should be found within the explored parametric domain, as it will be shown later by the global collapse of the numerical data cloud around the equation (3). In order to validate the coupled scaling relations derived at the dripping-jetting transition, we will conduct a comprehensive numerical study where both base flows and their global stability are evaluated (Fig. 2). Given that it is possible to define a steady surface charge density σ_e at the liquid interface $r = F(z)$, the leaky-dielectric model framework [22] is the best approach for the electrical modeling of our configuration, successfully applied on previous studies on pure electrospray in the cone-jet mode [23]. In the bulk, we have the dimensionless axisymmetric Navier-Stokes equations for the pressure $p^{(j)}(r,z;t)$ and velocity $\mathbf{v}^{(j)}(r,z;t) = u^{(j)}(r,z;t)\mathbf{e_r} + w^{(j)}(r,z;t)\mathbf{e_z}$, where r and z are the radial and axial coordinates, respectively. Likewise, the superscripts $j = \ell$ and g refer to the liquid and gas phases, respectively and the subscripts t, r and z stand for the corresponding partial derivatives for the variables involved. So, one reads

$$\nabla \cdot \mathbf{v}^{(j)} = 0, \tag{4}$$

$$\frac{\partial \mathbf{v}^{(j)}}{\partial t} + \rho^{\delta_{jg}}(\mathbf{v}^{(j)} \cdot \nabla)\mathbf{v}^{(j)} = -\nabla p^{(j)} + \mu^{\delta_{jg}} C \nabla^2 \mathbf{v}^{(j)}, \tag{5}$$

where $C = (2\mu_\ell^2/\rho_\ell \sigma D_i)^{1/2}$ is the Ohnesorge number of the liquid, t is the time and δ_{ij} is the Kronecker delta. As the Bond number $Bo = \rho_\ell g D_i/2\sigma \ll 1$ and the Froude number $Fr = v/(gD_i)^{1/2} \gg 1$, we can neglect gravitational effects along the fluid domain. Additionally, the electrical potential has to fulfill the Laplace equations

$$\nabla^2 \phi^{(j)} = 0 \tag{6}$$

Given a potential solution, the electric field at both sides of the jet surface is

$$E_k^{(j)} = \frac{F_z^{\delta_{k,n}} \phi_z^{(j)} - F_z^{(1-\delta_{k,n})} \phi_r^{(j)}}{(1+F_z^2)^{1/2}}, \tag{7}$$

where the subscripts $k = n$ and s denote the normal and shear directions, respectively. Besides, by the imposition of the kinematic compatibility and the balance of tangential and normal stresses on the interface, one reads

$$F_t + F_z w^{(\ell)} - u^{(\ell)} = F_t + F_z w^{(g)} - u^{(g)} = 0 \tag{8}$$

$$\sum_j^{\ell,g} (-1)^{\delta_{jg}} \{\mu^{\delta_{jg}} C[(1-F_z^2)(w_r^{(j)} + u_z^{(j)}) + 2F_z(u_r^{(j)} - w_z^{(j)})] - (-1)^{\delta_{jg}} \frac{1}{2}\sigma_e E_s^{(j)}\} = 0 \tag{9}$$

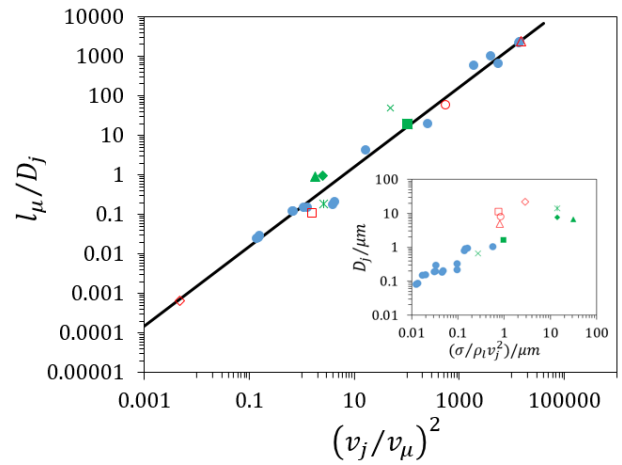

(a)

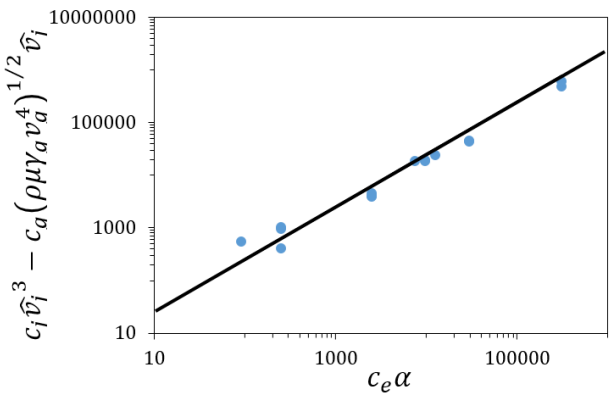

(b)

FIG. 3. (a) Critical points from the global stability analysis (blue circles), $(v_j/v_\mu)^2 = c_d l_\mu/D_j$ for $c_d = 11.4$ (solid line) with $R^2 = 0.973$. Experimental data from the literature for both flow focusing (FF) [24] and electrospray (ES) [19] are also plotted: 500-cSt Silicone Oil (FF, hollow red triangle), 100-cSt Silicone Oil (FF, hollow red circle), 5-cSt Silicone Oil (FF, hollow red square), Water (FF, hollow red diamond), 1-decanol (ES, green triangle) 1-octanol $D_i = 210$ μm (ES, green diamond), 1-octanol $D_i = 1100$ μm (ES, green star), 3-ETG + LiCa 0.00005M (ES, green square), 3-ETG + LiCa 0.0005M (ES, green cross). The embedded figure shows the dimensional relation rated to micrometers (b) Power balance equation (solid line) and critical stability points around it (blue circles) with $R^2 = 0.966$.

$$\sum_j^{\ell,g}((-1)^{\delta_{jg}} p^{(j)} + \frac{FF_{zz} - 1 - F_z^2}{F(1+F_z^2)^{3/2}} - \frac{1}{4}[2(-\beta)^{\delta_{j\ell}}(E_n^{(j)})^2 + (\beta-1)(E_s^{(j)})^2] - \frac{2\mu^{\delta_{jg}} C[u_r^{(j)} - F_z(w_r^{(j)} + u_z^{(j)}) + F_z^2 w_z^{(j)}]}{1+F_z^2}) = 0 \tag{10}$$

where $\chi = 2L_t/D_i$ is the electric Bond number and $\beta = \epsilon/\epsilon_o$. Considering both the jump condition for the normal electric field and the charge conservation at the

free surface, we obtain

$$\sigma_e = E_n^{(g)} - \beta E_n^{(\ell)} \tag{11}$$

$$\frac{\partial \sigma_e}{\partial t} + \frac{F_z u^{(\ell)} + w^{(\ell)}}{1+F_z^2}\sigma_{ez} - \frac{\sigma_e}{1+F_z^2}[u_r^{(\ell)} + F_z^2 w_z^{(\ell)} - F_z(u_z^{(\ell)} + w_r^{(\ell)})] = \alpha E_n^{(\ell)}, \tag{12}$$

At the inlet section z=0, we set a flat profile for the gaseous stream $U_g = 4\mu_g Re_g/\rho_g \pi D_g^{(h)}$ and a Hagen-Poiseuille parabolic profile $w^{(\ell)} = 8Q_\ell/(\pi D_i^2 v_c)(1-r^2)$ for the liquid phase. Previous flow profiles evolve along the domain downstream, drawing their respective boundary layers. Besides, the non-slip boundary condition is imposed at the solid walls and by simplification of the electric problem $\phi^i = \phi^o = \chi^{1/2}$. We prescribe the standard regularity conditions $\phi_r^i = u^{(\ell)} = w_r^{(\ell)} = 0$ at the symmetry z-axis, and outflow conditions $u_z^{(j)} = w_z^{(j)} = F_z = 0$ at $z = L_z$. As boundary conditions for the electrical potential at $r = L_r$, we assume an approximated analytical solution [25] successfully used in pure electrospray simulations [23],[17]

$$\phi_1(r', z') = \frac{-\chi^{1/2} K_v \ln\left\{\frac{[r'^2+(1-z')^2]^{1/2}+(1-z')}{[r'^2+(1+z')^2]^{1/2}+(1+z')}\right\}}{\ln(8H/D_i)}, \tag{13}$$

together with a logarithmic decreasing of the voltage in the radial direction at $z = 0$ and $D_i/2 < r < L_r$. The fluid domain is radially discretized via Chebyshev spectral collocation technique with 12 and 50 points for the liquid and gas domains, respectively, and through a fourth-order finite differences scheme for the longitudinal coordinate with 751 points. Once the numerical model is established, it is possible to obtain both the non-linear response and the eigenvalue problem to evaluate the global stability analysis of a basic flow with the same equation framework [26]. This allows us to capture the critical points of the dripping-jetting transition instead of classical spatio-temporal stability analysis that overestimates Q_{min} [27]. In order to calculate the linear global modes, we can assume a temporal dependence of a certain hydrodynamical variable $U(r,z;t) = U_o(r,t) + \eta\delta U(r,z)$ ($\eta \ll 1$), where $U_o(r,t)$ and $\delta U(r,z)$ are the steady flow and the eigenmode, respectively. This yields a complex eigenfrequency spectrum $\omega = \omega_r + i\omega_i$ and their corresponding eigenmodes δU as a function of the governing parameters. If the highest imaginary frequency is positive, then the system turns out asymptotically unstable [28]. An accurate validation demands an exhaustive exploration of the dimensionless parameters involved in the problem, namely $C \in [0.01234, 3.3242]$, $\chi \in [0, 12]$, $\alpha \in [13, 124479]$, $\beta \in [10, 50]$, $\mu \in [0.00016, 0.01625]$, $\rho \in [0.00104167, 0.0015625]$, $Re_g \in [0, 150]$, $U_\ell \in [0.0015, 0.02]$. From such an exploration we determined that both scaling relations collapse the numerical points with a remarkable agreement (Fig. 3), leading to the

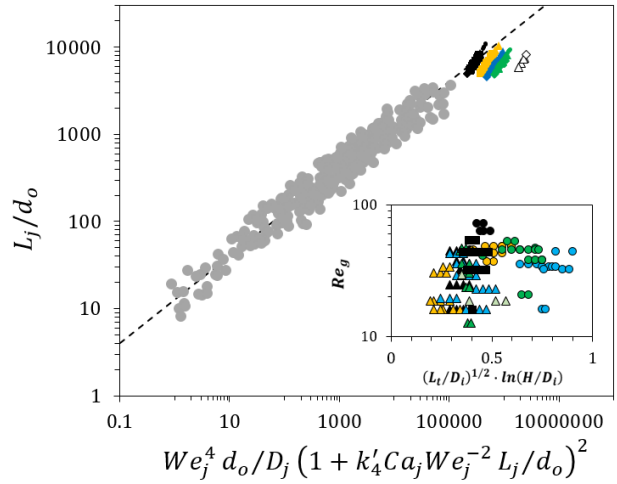

FIG. 4. Gañán-Calvo *et al.* jet length scaling law (dashed line) and their supporting experimental data (grey) [29] together with experimental realizations for this aero-electro configuration (color). In the embedded figure, the experimental points collected are plotted in terms of the gaseous Reynolds number and the dimensionless voltage. Mark color: $We_\ell = 6.24$ (black), 10.80 (yellow), 15.28 (blue), 19.72 (green), 44.11. Mark shape: $\left\{\widehat{H_p}, \Upsilon_g\right\} = \{0.326, 1.245\}$ (circle), $\{0.7, 1.98\}$ (triangle), $\{0, 0.847\}$ (square) $\{0, 1.779\}$ (diamond).

constants $c_d = 11.4$, $c_e = 2.58$, $c_j = 0.52$ and $c_g = 24.8$. Interestingly, we also find a generality for both flow focusing and electrospray, comparing our prediction to several dripping-jetting experiments from the literature, finding an excellent degree of matching. These results may suggest a common origin for the dripping-jetting instability of cone-jet configurations.

We now focus on conditions and parameters relevant for SFX experiments. In particular, we use a liquid (12 % water, 88 % glycerol doped with KCl) with $\rho_\ell = 1050$ kg/m^3, $\mu_\ell = 120$ mPa·s, $\sigma = 0.065$ N/m, $K = 0.1$ S/m and a flow rate ranging from 0.1 to 5 μL/min carefully fed from a syringe pump (CETONI, neMESYS 600). The voltage is applied onto the liquid through a metal wire connected upstream to a high voltage power supply (FUG HCP 35-20000) and the grounded electrode is placed at $H = 1.9\ mm$. The gas flow is pure nitrogen N_2, which is controlled via a pressure regulator upstream (SMC, IR2000-F02) and measured by a flow meter (Bronkhorst, EL-FLOW). A high-vacuum discharge ambient gas is kept at a pressure of about 10^{-3} Pa using vacuum pumps (Pfeiffer Vacuum). The nozzle fabrication by means of a laser lithography nano 3D printer (Nanoscribe GmbH, Photonic Professional GT) [30] allowed us to accurately explore the influence of the nozzle geometry in terms of $\widehat{H_p} = H_p/D_i$ and Υ_g for $D_i = 40\ \mu m$ (Fig. 4). A parametric island for steady jetting was found, with stable points for $We_\ell \approx 45$. This entails a potential increase of 50 % over the maximum jet speed of both flow fo-

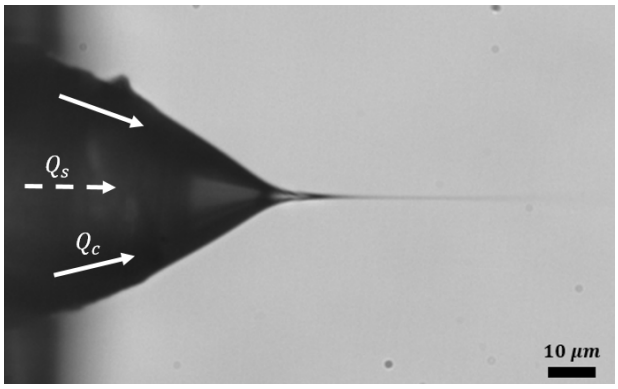

FIG. 5. Co-axial, miscible cone-jet. The sample (pure water) is fed from a capillary tube of 30 μm of diameter, placed at 60 μm upstream from the protruded tip. Conditions: $Q_c =$ 300 nL/min, $Q_s =$ 50 nL/min, $\Delta V =$ 2400 V, $Q_{mg} =$ 1.86 mg/min, $\widehat{H_p} = 0.7$, $\Upsilon_g = 1.96$, $D_j \approx 260$ nm and $v_j \approx 110$ m/s.

cusing and pure electrospray at their non-axisymmetric limit $We_\ell \sim 20$. Apart from jet steadiness, jet length also plays a major role for SFX application. This motivates a description of the jet length in terms of the governing parameters. In this regard, we use a jet length scaling recently derived for steady jetting of mechanical means [29] and expressed as

$$\frac{L_j}{d_o} = k_3^{1/2} We_\ell^2 \left(\frac{d_o}{D_j} \left(1 + k_4^{'} Ca_\ell We_\ell^{-2} \frac{L_j}{d_o} \right) \right)^{1/2} \quad (14)$$

where $d_o = \sigma/\Delta P$, $Ca_\ell = \mu_\ell v_j/\sigma$, $k_3 \approx 163$ is an universal factor and $k_4^{'}$ is a constant that depends on the type of ejector. Here, we take the same value than that for gas focused jets $k_4^{'} = 0.175$. To adapt properly that model to our system, we assume a negligible influence of ΔV at first-order, given its narrow range at steady jetting (Fig. 4). Thus, we use an equivalent liquid pressure $\Delta P \sim \Delta P_{ES} + \psi \Delta P_g$ including both electrical ΔP_{ES} and gas pressure ΔP_g, according to classical gas discharge through apertures. Despite that most of our experimental realizations properly fit the adapted scaling law for $\psi = 25$, the upper limit found for flow focused jets is exceeded (Fig. 4). Additionally, given a ΔP_g, the nozzle geometry does not show any significant influence over the jet length.

Lastly, we show the possibility of delivering two miscible liquids with a double configuration. The inner liquid (s) can be steadily and coaxially issued through an outer liquid (c) at liquid flow rates even smaller than what the physical limit dictates for the same liquid (s) in a single configuration. For instance, we generate steady jets for $Q_c/Q_s \in (1, 6)$, delivering pure water through the liquid previously mentioned. Interestingly, we found conditions for steady jets with $D_j \approx 260$ nm and $v_j \approx 110$ m/s, values obtained by using our model with a total flow rate $Q_\ell = Q_c + Q_s$ of a liquid equivalent to the resulting mixture at the ratio $Q_c/Q_s = 6$ (Fig. 5).

This work was supported by the Ministerio de Economía y Competitividad (Spain), Plan Estatal 2013-2016 Retos, project DPI2016-78887-C3-1-R, and the German Science Foundation (DFG) through the Gottfried Wilhelm Leibniz programme.

[1] J. Eggers and E. Villermaux, Rep. Prog. Phys. **71**, 036601 (2008).
[2] J. B. Fenn, M. Mann, C. K. Meng, S. F. Wong, and C. M. Whitehouse, Science **246**, 64 (1989).
[3] Z. Takáts, J. M. Wiseman, B. Gologan, and R. G. Cooks, Science **306**, 471 (2004).
[4] A. Jaworek, J. Mater. Sci. **42**, 266 (2007).
[5] H. N. Chapman *et al.*, Nature **470**, 73 (2011).
[6] A. M. Gañán-Calvo, Phys. Rev. Lett. **80**, 285 (1998).
[7] D. P. DePonte, U. Weierstall, K. Schmidt, J. Warner, D. Starodub, J. C. H. Spence, and R. B. Doak, J. Phys. D: Appl. Phys. **41**, 195505 (2008).
[8] D. Obertuer, J. Knoška, and M. O. Wiedorn *et al.*, Scientific Reports **7**, 44628 (2017).
[9] R. Sierra *et al.*, Acta Crystallographica Section D: Biological Crystallography **68**, 1584 (2012).
[10] R. Sierra *et al.*, Nature Methods **13**, 59 (2015).
[11] C. Pellegrini, A. Marinelli, and S. Reiche, Rev. Mod. Phys. **88**, 102601 (2016).
[12] R. Neutze, R. Wouts, D. V. D. Spoel, E. Weckert, and J. Hajdu, Nature **406**, 752 (2000).
[13] M. O. Wiedorn *et al.*, IUCRJ **5**, 574 (2018).
[14] M. O. Wiedorn *et al.*, Nat. Commun. **9**, 3487 (2018).
[15] C. A. Stan *et al.*, Nature Physics **12**, 966 (2016).
[16] A. M. Gañán-Calvo and J. M. Montanero, Phys. Rev. E **79**, 066305 (2009).
[17] A. M. Gañán-Calvo, J. M. López-Herrera, M. A. Herrada, A. Ramos, and J. M. Montanero, Journal of Aerosol Science **125**, 32 (2018).
[18] F. Cruz-Mazo, M. A. Herrada, A. M. Gañán-Calvo, and J. M. Montanero, J. Fluid Mech. **832**, 329 (2017).
[19] A. Ponce-Torres, N. Rebollo-Muñoz, M. A. Herrada, A. M. Gañán-Calvo, and J. M. Montanero, J. Fluid Mech. **857**, 142 (2018).
[20] A. M. Gañán-Calvo, Phys. Rev. Lett. **79**, 217 (1997).
[21] A. M. Gañán-Calvo, J. Fluid Mech. **507**, 203 (2004).
[22] D. A. Saville, Annu. Rev. Fluid Mech. **29**, 27 (1997).
[23] M. A. Herrada, J. M. López-Herrera, A. M. Gañán-Calvo, E. J. Vega, J. M. Montanero, and S. Popinet, Phys. Rev. E **86**, 026305 (2012).
[24] A. J. Acero, C. Ferrera, J. M. Montanero, and A. M. Gañán-Calvo, J. Micromech. Microeng. **22**, 065011 (2012).
[25] A. M. Gañán-Calvo, J. C. Lasheras, J. Dávila, and A. Barrero, J. Aerosol Sci. **25**, 1121 (1994).
[26] M. A. Herrada and J. M. Montanero, J. Comput. Phys. **306**, 137 (2016).
[27] A. M. Gañán-Calvo, Phys. Rev. Lett. **98**, 134503 (2007).
[28] V. Theofilis, Annu. Rev. Fluid Mech. **43**, 319 (2011).
[29] A. M. Gañán-Calvo *et al.*, Phys. Rev. Lett. , submitted (2018).

[30] G. Nelson *et al.*, Optics Express **24**, 11515 (2016).